Journal of Sound and Vibration (1997) **204**(3), 459–476

STEADY-STATE RESPONSE OF ACOUSTIC CAVITIES BOUNDED BY PIEZOELECTRIC COMPOSITE SHELL STRUCTURES

I. KALJEVIĆ†

AYT Corporation, 2001 *Aerospace Parkway Brook Park*, *OH* 44142, *U.S.A.*

AND

D. A. SARAVANOS

Ohio Aerospace Institute, 22800 *Cedar Point Road*, *Cleveland*, *OH* 44142, *U.S.A.*

(*Received* 22 *July* 1996, *and in final form* 13 *December* 1996)

A formulation to calculate the coupled response of composite shells with embedded piezoelectric layers and an enclosed acoustic fluid is presented in this paper. The methodology consists of three parts: (1) a formulation for the electro-mechanical response of piezoelectric shells; (2) a formulation for the three-dimensional acoustic response of the enclosed fluid; and (3) the combination of the formulations (1) and (2) to calculate the coupled smart structure-acoustic fluid response. A recently developed mixed field laminate theory is adapted for the analysis of piezoelectric shells. The theory combines the first order shear theory kinematic assumptions with a layer-wise approximation for the electric potential. Shell geometry is described in an orthogonal curvilinear co-ordinate system and general piezoelectric material descriptions and laminate configurations are considered. A boundary element formulation is developed to calculate the acoustic response of the enclosed fluid. Quadratic conforming boundary elements are used to discretize the fluid boundary. Advanced numerical integration techniques are employed to calculate singular elements in boundary element matrices. The treatment of distributed acoustic sources is also presented. A formulation to calculate the coupled fluid-structure response is also developed. Relations between the structural and acoustic variables on the structure-fluid interface are utilized to generate the coupled system of equations in terms of the kinematic shell variables and acoustic pressures on the fluid boundary. The convergence of the present developments is established by studying a circular cylindrical shell with an attached piezoelectric layer. The coupled response is investigated for various types of mechanical loads and active voltage patterns.

1. INTRODUCTION

The application of composite materials with embedded piezoelectric sensors and actuators for improving the performance, versatility and reliability of aeropropulsion and aerospace components is receiving growing attention. One such area where the unique properties of smart piezoelectric structures can be utilized is the active modification of acoustic fields in fluids enclosed by smart structures, which may result in the reduction of aircraft noise in the engine or the cabin [1, 2]. Yet, only few attempts to utilize active piezoelectric structures in noise control have appeared recently, which address the problem of a three-dimensional rigid enclosure of hexahedral shape with a flexible wall made of

† To whom all correspondence should be addressed, presently at: ANSYS, Inc, Southpointe, 275 Technology Drive, Canonsburg, PA 15317, U.S.A.

0022–460X/97/280459 + 18 $25.00/0/sv960911

piezoelectric material [3–5]. Although these studies provide some understanding of the coupled smart structure-acoustic fluid behavior, they were neither intended nor can be used for the treatment of realistic engineering problems. In order to successfully utilize piezoelectric smart structures in noise reduction, the coupled response of the fluid surrounded by a smart shell structure of arbitrary shape, lamination and general material properties subjected to a variety of external influences needs to be formally predicted. To the authors' best knowledge such capability does not seem to be presently available. Consequently, the present paper attempts to remedy this void in current technology by presenting a theoretical formulation and its numerical implementation for calculating the coupled smart shell structure-acoustic fluid response.

The coupled smart structure-acoustic fluid analysis consists of three parts: (1) analysis of layered composite structures of arbitrary shapes that contain embedded piezoelectric materials; (2) acoustic response of the enclosed fluid; (3) coupling of the fluid and structure responses. The work in each of these three areas is reviewed in the following paragraphs. The development of the combined method for the analytical and numerical solution of the coupled problem is new and is presented herein.

The majority of theories available for analyzing piezoelectric shell structures have used classical or first order shear kinematic assumptions with equivalent force representations of induced strain in a piezoelectric laminate [6–9]. Such approaches effectively neglect the piezoelectric coupling on the structure level. Layer-wise formulations that explicitly define electric potentials as unknown variables were developed recently by Heyliger *et al*. [10] and Tzou and Ye [11]. While these formulations are capable of providing accurate results, they are essentially three-dimensional techniques leading to a large number of degrees of freedom in the resulting system of equations. This may result in computationally expensive analyses when a shell is coupled with the acoustic medium. A so called "mixed-field" piezoelectric shell theory and the corresponding finite element, recently developed by Saravanos [12], are employed in the present development. The theory combines the first order shear deformation approximation to model the strain field and a layer-wise approximation of the electric potentials. A general material description is incorporated into stress-strain relations, and shells of arbitrary shapes and laminate configurations are considered. As has been shown in the literature [13], the single-layer theories provide accurate global responses of the thin and moderately thick composite structures without interfacial cracks and delaminations. Such an accuracy is sufficient for applications anticipated for the present developments, such as noise reduction. The model size is significantly reduced, while the piezoelectric coupling is preserved. The problems associated with relative dimensions of the elements that may lead either to locking or to ill-conditioned system matrices are eliminated.

In order to study the effects of the active structure on noise in the acoustic enclosure, a formulation to calculate the acoustic pressures in the enclosed fluid needs to be developed. The boundary element method is used in the present study to model the acoustic response of the fluid, because the unknown variables are introduced only on the boundary leading to a significantly smaller system of equations. Quadratic conforming boundary elements are used to discretize the boundary. Advanced numerical integration schemes [14, 15] are used to calculate weakly singular terms while the strongly singular terms in the boundary element matrix are calculated indirectly. Two distinct treatments of distributed acoustic sources are presented. A domain integration technique, similar to that devised for two-dimensional problems [16], is devised for arbitrary sources, and the particular integral method [17, 18] is employed for sources prescribed using analytical expressions.

A formulation to calculate the coupled fluid-structure response is developed next. Special attention has been paid in the literature to the coupling of fluid and structural responses [19–22]. Depending on the desired application, two distinct methodologies were utilized [21]: the structural variable methodology, where the unknown acoustic pressures are eliminated to cast the system of equations in terms of structural variables only; and the fluid variable methodology where the structural variables are eliminated in favor of acoustic pressures. A different procedure was recently proposed by Rajakumar *et al*. [23] where both the fluid and the structural variables are retained in the final systems of equations. All of the above formulations, however, have assumed that the entire fluid boundary is in contact with the structure. In this paper, it is assumed that only portions of the shell surface and the fluid boundary are in contact with each other. Relations between the structural and acoustic variables on the interface are utilized to generate the coupled system of equations. Condensation of electric variables is performed and the final system of equations is written in terms of the kinematic shell variables and acoustic pressures on the fluid boundary. The coupled response is calculated for (1) mechanical loadings, (2) applied electrical potentials, and (3) distributed acoustic sources. The unknown electric potentials are then obtained from shell displacements using the electric condensation equations. The acoustic pressures in the interior of the fluid domain are calculated using the corresponding boundary values.

Numerical results are presented for a closed cylindrical ring with a piezoelectric layer. Convergence studies are performed to validate the formulation for the coupled response. Additional studies investigate the acoustic pressures in the enclosed fluid induced by external mechanical loadings and applied electric potentials.

2. MIXED-FIELD LAMINATE THEORY FOR PIEZOELECTRIC SHELLS

The mixed field laminate theory for analyzing composite piezoelectric shells is briefly reviewed in order to introduce the notation and assumptions used throughout this study. Additional details may be found in reference [12]. A composite laminated shell, as shown in Figure 1, is considered. The geometric configuration of the shell is described in a Cartesian co-ordinate system $Oxyz$. It is assumed that the position vector of an arbitrary point within the shell, $\mathbf{r} = \{x\ y\ z\}^{\mathrm{T}}$, may be expressed as

$$\mathbf{r}(\alpha, \beta, \gamma) = \mathbf{r}_o(\alpha, \beta) + \gamma\hat{\gamma}, \tag{1}$$

where the vector $\mathbf{r}_o(\alpha, \beta)$ defines the reference surface A_o, α and β are orthogonal curvilinear co-ordinates defined on A_o, and γ is the third co-ordinate corresponding to the

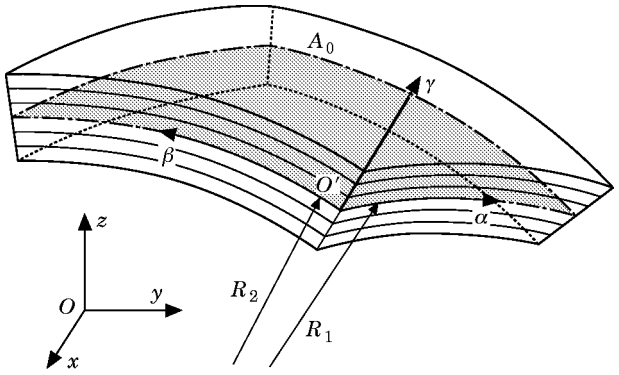

Figure 1. Curvilinear piezoelectric configuration and co-ordinate systems.

unit vector γ that is orthogonal to the reference surface. The shell consists of a number of plies that are parallel to the reference surface A_o and are made of piezoelectric or composite materials with arbitrary fiber orientations. The constitutive relations in each layer are defined in the curvilinear co-ordinate system $O'\alpha\beta\gamma$ and are given as

$$\{\boldsymbol{\sigma}\} = [\mathbf{C}]\{\boldsymbol{S}\} - [\mathbf{e}]\{\boldsymbol{E}\}, \qquad \{\boldsymbol{D}\} = [\mathbf{e}]^{\mathrm{T}}\{\boldsymbol{S}\} + [\boldsymbol{\varepsilon}]\{\boldsymbol{E}\}, \tag{2a, b}$$

where $\{\boldsymbol{\sigma}\}^{\mathrm{T}} = \{\sigma_{\alpha\alpha}\ \sigma_{\beta\beta}\ \sigma_{\gamma\gamma}\ \sigma_{\beta\gamma}\ \sigma_{\gamma\alpha}\ \sigma_{\alpha\beta}\}$ and $\{\boldsymbol{S}\}^{\mathrm{T}} = \{S_{\alpha\alpha}\ S_{\beta\beta}\ S_{\gamma\gamma}\ S_{\beta\gamma}\ S_{\gamma\alpha}\ S_{\alpha\beta}\}$ are the stress and strain vectors, respectively; $\{\boldsymbol{E}\} = \{E_\alpha\ E_\beta\ E_\gamma\}$ is the vector of electric field; $\{\boldsymbol{D}\} = \{D_\alpha\ D_\beta\ D_\gamma\}$ is the vector of electric displacements; $[\mathbf{C}]$ is the stiffness matrix of the material; $[\mathbf{e}]$ is the matrix of piezoelectric properties; and $[\boldsymbol{\varepsilon}]$ is the matrix of dielectric properties. Governing equations are derived using Hamilton's principle which is written as [24]

$$\int_{t_o}^{t} \mathrm{d}t \int_V [\rho\{\delta u\}^{\mathrm{T}}\{\ddot{u}\} + (\{\delta S\}^{\mathrm{T}}\{\sigma\} - \{\delta E\}^{\mathrm{T}}\{\boldsymbol{D}\})]\,\mathrm{d}V - \int_{t_o}^{t} \mathrm{d}t \int_\Gamma (\{\delta u\}^{\mathrm{T}}\{\bar{\tau}\} - \delta\phi\bar{\zeta})\,\mathrm{d}\Gamma = 0, \tag{3}$$

where V is the shell domain bounded by the contour Γ; δ denotes variation; $(\dot{})$ denotes time differentiation; ρ is the mass density of the material; $\{\bar{\tau}\}$ are prescribed surface tractions; and $\bar{\zeta}$ is the prescribed surface charge. The displacement field is approximated using first-order shear deformation assumptions. The components of the displacement vector at location $\mathbf{r}$ and a time instant t are given as

$$u(\alpha, \beta, \gamma, t) = u^o(\alpha, \beta, \gamma, t) + \gamma\psi_\alpha(\alpha, \beta, t), \qquad v(\alpha, \beta, \gamma, t) = v^o(\alpha, \beta, \gamma, t) + \gamma\psi_\beta(\alpha, \beta, t), \tag{4a, b}$$

$$w(\alpha, \beta, \gamma, t) = w^o(\alpha, \beta, \gamma, t), \tag{4c}$$

where superscript o denotes the values on the reference surface A_o, and ψ_α and ψ_β are rotation angles with respect to axes α and β. The components of the strain vector $\{\boldsymbol{S}\}$ are given in reference [12]:

$$S_i(\alpha, \beta, \gamma, t) = S_i^o(\alpha, \beta, \gamma, t) + \gamma k_i(\alpha, \beta, t), \qquad i = 1, 2, 6; \qquad S_3(\alpha, \beta, \gamma, t) = 0; \tag{5a, b}$$

$$S_i(\alpha, \beta, \gamma, t) = S_i^o(\alpha, \beta, t), \qquad i = 4, 5; \tag{5c}$$

where S_i^o, $i = 1, 2, \ldots, 6$ are the strain components at the reference surface:

$$S_1^o = S_{\alpha\alpha}^o = (1/g_{11}^o)(u_{,\alpha}^o + (g_{11,\beta}^o/g_{22}^o)v^o) + w^o/R_1, \tag{6a}$$

$$S_2^o = S_{\beta\beta}^o = (1/g_{22}^o)(v_{,\beta}^o + (g_{22,\alpha}^o/g_{11}^o)u^o) + w^o/R_2, \tag{6b}$$

$$S_6^o = S_{\alpha\beta}^o = 1/g_{11}^o(v_{,\alpha}^o - (g_{11,\beta}^o/g_{22}^o)u^o) + (1/g_{22}^o)(u_{,\beta}^o - (g_{22,\alpha}^o/g_{11}^o)v^o), \tag{6c}$$

$$S_4^o = S_{\beta\gamma}^o = \psi_\beta + w_{,\beta}^o/g_{22}^o - v^o/R_2, \qquad S_5^o = S_{\gamma\alpha} = \psi_\alpha + w_{,\alpha}^o/g_{11}^o - u^o/R_1, \tag{6d, e}$$

where $g_{11}^o = \sqrt{x_{o,\alpha}^2 + y_{o,\alpha}^2 + z_{o,\alpha}^2}$; $g_{22}^o = \sqrt{x_{o,\beta}^2 + y_{o,\beta}^2 + z_{o,\beta}^2}$; and the curvatures k_1, k_2, and k_6 are respectively given as

$$k_1 = k_{\alpha\alpha} = (1/g_{11}^o)(\psi_{\alpha,\alpha} + (g_{11,\beta}^o/g_{22}^o)\psi_\beta), \quad k_2 = k_{\beta\beta} = (1/g_{22}^o)(\psi_{\beta,\beta} + (g_{22,\alpha}^o/g_{11}^o)\psi_\alpha), \tag{7a, b}$$

$$k_6 = k_{\alpha\beta} = (1/g_{11}^o)(\psi_{\beta,\alpha} - (g_{11,\beta}^o/g_{22}^o)\psi_\alpha) + (1/g_{22}^o)(\psi_{\alpha,\beta} - (g_{22,\alpha}^o/g_{11}^o)\psi_\beta). \tag{7c}$$

For the approximation of the electric field, the laminate is subdivided into $N-1$ discrete layers and linear variation of electric potentials is assumed in each discrete layer. The

minimum number of discrete layers is equal to the number of piezoelectric layers in the laminate. The electric potential is approximated as

$$\phi(\alpha, \beta, \gamma, t) = \sum_{j=1}^{N} \phi^j(\alpha, \beta, t)\bar{N}^j(\gamma), \tag{8}$$

where $\phi^j(\alpha, \beta, t)$ is the value of the electric potential at $\gamma = h_j$ [12], and $\bar{N}^j(\gamma)$, $j = 1, 2, \ldots, N$, are through-thickness interpolation functions. The components of the vector of the electric field can now be written as

$$E^j_\alpha = -\phi^j_{,\alpha}/g^o_{11}, \qquad E^j_\beta = \phi^j_{,\beta}/g^o_{22}, \qquad E^j_\gamma = -\phi^j. \tag{9}$$

Equations (4) and (8) are employed to devise a finite element for the approximate analysis of composite piezoelectric shells. The element is defined on the reference surface A_o, and is assumed to have M_s nodes. Five kinematic degrees of freedom, three displacements u_j, v_j and w_j, and two rotations $\psi_{\alpha j}$ and $\psi_{\beta j}$, together with N electric potentials ϕ^n_j corresponding to interfaces of $(N-1)$ layers, are defined at each node. The kinematic and electric variables are approximated in the surface A_o as

$$\chi^o(\alpha, \beta, t) = \sum_{i=1}^{M_s} N^i(\alpha, \beta)\chi^o_i(t), \qquad \phi^m(\alpha, \beta, t) = \sum_{i=1}^{M_s} N^i(\alpha, \beta)\phi^m_i(t), \qquad m = 1, 2, \ldots, N, \tag{10a, b}$$

where χ denotes a kinematic degree of freedom and $N^i(\alpha, \beta)$, $i = 1, 2, \ldots, M_s$, are element interpolation functions. Equations (6), (9), and (10) are introduced into equation (3) to obtain the discretized system of equation for the piezelectric composite shell as

$$\begin{bmatrix} [\mathbf{M}_{uu}] & [\mathbf{0}] \\ [\mathbf{0}] & [\mathbf{0}] \end{bmatrix} \begin{Bmatrix} \{\ddot{\boldsymbol{U}}(t)\} \\ \{\ddot{\boldsymbol{\Phi}}(t)\} \end{Bmatrix} + \begin{bmatrix} [\mathrm{K}_{uu}] & [\mathrm{K}_{u\phi}] \\ [\mathrm{K}]_{\phi u} & [\mathrm{K}_{\phi\phi}] \end{bmatrix} \begin{bmatrix} \boldsymbol{U}(t)\} \\ \boldsymbol{\Phi}(t)\} \end{bmatrix} = \begin{bmatrix} \{\boldsymbol{P}(t)\} \\ \{\boldsymbol{Q}(t)\} \end{bmatrix}, \tag{11}$$

where $\{\mathbf{P}(t)\}$ is the equivalent load vector due to mechanical loads and $\{\mathbf{Q}(t)\}$ represents contributions of applied electric charges. Expressions for the matrices appearing in equation (11) are given in reference [12].

3. BOUNDARY ELEMENT FORMULATION FOR THREE-DIMENSIONAL ACOUSTICS

A three-dimensional boundary element formulation to calculate the acoustic pressure in a compressible fluid subjected to harmonic disturbances is presented in this section. For such a case, the wave equation is reduced to the Helmholtz equation [25],

$$\nabla^2 p + k^2 p + \Psi = 0; \tag{12}$$

where p is the amplitude of time harmonic pressure; $k = \omega/c$ is the wave number; ω is the angular frequency of the oscillations; and Ψ is the distributed acoustic source. The Kirchhoff–Helmholtz integral representation of equation (12) is obtained as [26]

$$c(\boldsymbol{\zeta})p(\boldsymbol{\zeta}) = \int_\Gamma [G(\mathbf{x}, \boldsymbol{\zeta})p_n(\mathbf{x}) - F(\mathbf{x}, \boldsymbol{\zeta})p(\mathbf{x})]\, \mathrm{d}\Gamma(\mathbf{x}) + \int_\Omega G(\mathbf{z}, \boldsymbol{\zeta})\Psi(\mathbf{z})\, \mathrm{d}\Omega(\mathbf{z}), \tag{13}$$

where Ω is the domain of the fluid bounded by the contour Γ; $\mathbf{x}$ and $\boldsymbol{\zeta}$ are two points that lie on the boundary; $\mathbf{z}$ denotes a location within the domain Ω; p_n is the normal derivative

of the acoustic pressure; $c(\boldsymbol{\zeta})$ is the corner tensor term [14]; and $G(\mathbf{x}, \boldsymbol{\zeta})$ and $F(\mathbf{x}, \boldsymbol{\zeta})$ are the boundary element kernels that are defined as

$$G(\mathbf{x}, \boldsymbol{\zeta}) = (1/4\pi k)(\mathrm{e}^{\mathrm{i}kr}/r), \qquad F(\mathbf{x}, \boldsymbol{\zeta}) = (1/4\pi k)(\mathrm{e}^{\mathrm{i}kr}/r^3)(\mathrm{i}kr - 1)y_l n_l. \tag{14}$$

In equations (14), i is the imaginary unit; $r = |\mathbf{x} - \boldsymbol{\zeta}|$; $y_l = x_l - \zeta_l$, $l = 1, 2, 3$; repeated indices denote summation; and $\{\boldsymbol{n}\}^{\mathrm{T}} = [n_1 \ n_2 \ n_3]$ is the unit outward normal vector at the point $\mathbf{x}$ of the boundary. Equation (13) is rewritten as

$$c(\boldsymbol{\zeta})p(\boldsymbol{\zeta}) = \mathscr{I}(\boldsymbol{\zeta}) + \mathscr{J}(\boldsymbol{\zeta}), \tag{15}$$

where $\mathscr{I}(\boldsymbol{\zeta})$ and $\mathscr{J}(\boldsymbol{\zeta})$ denote the contour and volume integral on the right side of equation (13), respectively.

The boundary element discretization of equation (15) is now presented. The contour integral $\mathscr{I}(\boldsymbol{\zeta})$ is considered first. The boundary Γ is descretized into N_e quadratic, conforming boundary elements. The location of a point $\mathbf{x}$ within the boundary element is approximated as

$$x_i = \sum_{j=1}^{M_f} x_i^j N_j(\xi, \eta), \qquad i = 1, 2, 3, \tag{16}$$

where $N_j(\xi, \eta)$, $j = 1, 2, \ldots, M_f$ are interpolation functions, similar to those used in the finite element discretization; x_i^j are co-ordinates of element nodes; M_f is the number of nodes; and ξ and η are non-dimensional local co-ordinates. The unknown variables are approximated using expressions similar to equation (16). The integral $\mathscr{I}(\boldsymbol{\zeta}_m)$ is now written as

$$\mathscr{I}(\boldsymbol{\zeta}_m) = \sum_{i=1}^{N_e} \int_{\Gamma_i} \sum_{j=1}^{M_f} [G(\mathbf{x}, \boldsymbol{\zeta}_m)p_{nj} - F(\mathbf{x}, \boldsymbol{\zeta}_m)p_j]N^j(\xi, \eta)|J_i| \, \mathrm{d}\xi \, \mathrm{d}\eta, \qquad m = 1, 2, \ldots, M, \tag{17}$$

where $\boldsymbol{\zeta}_m$ is the position vector of the boundary element node, m; M is the total number of nodes resulting from the boundary element discretization; p_j and p_{nj} are nodal values of the acoustic pressure and its normal derivative; Γ_i denotes the domain of the boundary element i; and $|J_i|$ is the determinant of the Jacobian of the co-ordinate transformation given in equation (16). The integrals that appear in equation (17) are calculated using the advanced numerical integration scheme developed by Lachat and Watson [15]. The integration of the weakly singular [14] kernel $G(\mathbf{x}, \boldsymbol{\zeta}_m)$ is performed directly by subdividing the element into triangles which all contain the node $\boldsymbol{\zeta}_m$ as a vertex. The kernel $F(\mathbf{x}, \boldsymbol{\zeta}_m)$, however, is strongly singular and cannot be calculated directly when the node m belongs to the element being integrated. An indirect technique, devised originally for transient elastodynamics problems [27, 28], is used instead. The kernel $F(\mathbf{x}, \boldsymbol{\zeta}_m)$ is expressed as

$$F(\mathbf{x}, \boldsymbol{\zeta}_m) = \tilde{F}(\mathbf{x}, \boldsymbol{\zeta}_m) + F_x(\mathbf{x}, \boldsymbol{\zeta}_m); \tag{18}$$

where $\tilde{F}(\mathbf{x}, \boldsymbol{\zeta}_m) = F(\mathbf{x}, \boldsymbol{\zeta}_m) - F_c(\mathbf{x}, \boldsymbol{\zeta}_m)$ and $F_c(\mathbf{x}, \boldsymbol{\zeta}_m) = 1/(4\pi kr)$ is the fundamental solution for the three-dimensional potential problems. The modified kernel $\tilde{F}(\mathbf{x}, \boldsymbol{\zeta}_m)$ is not singular, and can be directly calculated. An indirect technique that utilizes a state of uniform unit potentials prescribed along the entire boundary of the object [14] is used to calculate strongly singular terms corresponding to the kernel $F_c(\mathbf{x}, \boldsymbol{\zeta}_m)$.

Calculations of the domain integral $\mathscr{J}(\boldsymbol{\zeta})$ are considered next. The domain Ω is divided into N_c volume cells, and the expression for the domain integral is written as

$$\mathscr{J}(\boldsymbol{\zeta}_m) = \sum_{i=1}^{M_c} \sum_{\Omega_i} G(\mathbf{z}, \boldsymbol{\zeta}_m) \Psi(\mathbf{z}) \, \mathrm{d}\Omega_i(\mathbf{z}). \tag{19}$$

The domain integral $\mathscr{J}(\boldsymbol{\zeta}_m)$ involves only known quantities. Thus, there is no need to impose compatibility of the interpolation functions either between the adjacent cells, or between the cells and the boundary elements allowing an integration scheme similar to that developed by Kaljević and Saigal [16] for integration of two-dimensional domains to be used. In this scheme, eight-node hexahedral cells are used to discretize the domain Ω. An analytical integration is employed to calculate weakly singular integrals that appear for cells that contain boundary nodes, and the standard Gauss integration is used for the non-singular integration.

Equation (15) is written for all boundary element nodes, and the standard boundary element assembly procedure [14] is applied to arrive to a system of equations given as

$$[\mathbf{F}]\{\boldsymbol{p}\} = [\mathbf{G}]\{\boldsymbol{p}_n\} + \{\boldsymbol{\Psi}\}, \tag{20}$$

where $\{\boldsymbol{p}\}$ is the vector of acoustic pressures defined at boundary element nodes; $\{\boldsymbol{p}_n\}$ is the vector of corresponding normal derivatives; $[\mathbf{G}]$ and $[\mathbf{F}]$ are boundary system matrices corresponding to contour integrals of kernels $G(\mathbf{x}, \boldsymbol{\zeta})$ and $F(\mathbf{x}, \boldsymbol{\zeta})$, respectively, and $\{\boldsymbol{\Psi}\}$ represents the contribution from distributed sources. After solving equation (20) for unknown quantities on the boundary, the values of acoustic pressures inside the domain can be calculated using equation (13) and setting $c(\boldsymbol{\zeta}) = 1$.

If the acoustic sources are prescribed by an analytical expression the domain integration may be avoided by utilizing the particular integral approach [17, 18]. The vector of distributed sources in this case can be expressed as

$$\{\boldsymbol{\Psi}\} = [\mathbf{F}]\{\bar{\boldsymbol{p}}\} - [\mathbf{G}]\{\bar{\boldsymbol{p}}_n\}, \tag{21}$$

where $\{\bar{\boldsymbol{p}}\}$ and $\{\bar{\boldsymbol{p}}_n\}$ are vectors of particular integral solutions of equation (12) for acoustic potential and corresponding normal derivative.

4. COUPLED SMART STRUCTURE—ACOUSTIC FLUID RESPONSE

A vibrating piezoelectric composite shell enclosing the acoustic fluid is considered in this section. Three families of state variables characterize the smart composite shell and acoustic fluid responses: (1) generalized mechanical displacements at finite element nodes; (2) electric potentials at piezoelectric layer interfaces; and (3) acoustic pressures on the boundary of the enclosed fluid. Considering that such comprehensive response may result in a large system of equatons, it is desirable to reduce the size of the system given in equation (11) by eliminating sensory electric potentials, $\{\boldsymbol{\Phi}_s\}$. The vector $\{\boldsymbol{\Phi}_s\}$ can be expressed as [12]

$$\{\boldsymbol{\Phi}_s(t)\} = [\mathbf{K}_{\phi\phi}^{ss}]^{-1}(\{\boldsymbol{Q}_s(t)\} - [\mathbf{K}_{\phi u}^{s}]\{\boldsymbol{U}(t)\} - [\mathbf{K}_{\phi\phi}^{sa}]\{\boldsymbol{\Phi}_a(t)\}), \tag{22}$$

where $\{\boldsymbol{\Phi}_a(t)\}$ is the vector of active potentials, and superscripts a and s denote blocks in the stiffness matrix corresponding to active and sensory potentials, respectively. Equation (22) is introduced into equation (11) to obtain the reduced structural system as

$$[\mathbf{M}]\{\ddot{\boldsymbol{U}}(t)\} + [\bar{\mathbf{K}}]\{\boldsymbol{U}(t)\} = \{\boldsymbol{P}(t)\} + \{\tilde{\boldsymbol{Q}}(t)\}, \tag{23}$$

where

$$[\bar{\mathbf{K}}] = [\mathbf{K}^s_{u\phi}][\mathbf{K}^{ss}_{\phi\phi}]^{-1}[\mathbf{K}^s_{\phi u}], \tag{24}$$

$$\{\tilde{\boldsymbol{Q}}(t)\} = [\mathbf{K}^s_{u\phi}][\mathbf{K}^{ss}_{\phi\phi}]^{-1}(\{[\mathbf{K}^{sa}_{\phi\phi}]\{\boldsymbol{\Phi}_a(t)\} - Q_s(t)\}) - [\mathbf{K}^a_{u\phi}]\{\boldsymbol{\Phi}_a(t)\}. \tag{25}$$

For the case of harmonic excitation of frequency ω, equation (23) is written as

$$[\mathbf{K}^*]\{\boldsymbol{U}\} = \{\boldsymbol{P}\} + \{\tilde{\boldsymbol{Q}}\}, \tag{26}$$

where $[\mathbf{K}^*] = -\omega^2[\mathbf{M}] + [\bar{\mathbf{K}}]$ and the vectors denote amplitudes of corresponding quantities.

The relations between the shell and fluid variables on the interface are now derived. The most general case where only portions of the shell and the fluid boundary are in contact with each other is considered. The shell surface Γ^s is divided into regions Γ_o and Γ^s_c, while the fluid boundary Γ^f consists of regions Γ^f_c and Γ_a. The regions Γ^s_c and Γ^s_f are equal to each other and represent the interface, Γ_c, between the fluid and the structure. The shell and fluid equations are partitioned such that the response variables corresponding to the surfaces mentioned above are grouped together, and are given as

$$\begin{bmatrix}[\mathbf{K}^*_{oo}] & [\mathbf{K}^*_{oc}]\\ [\mathbf{K}^*_{co}] & [\mathbf{K}^*_{cc}]\end{bmatrix}\begin{Bmatrix}\{\boldsymbol{U}_o\}\\ \{\boldsymbol{U}_c\}\end{Bmatrix} = \begin{Bmatrix}\{\boldsymbol{P}^q_o\} + \{\tilde{\boldsymbol{Q}}_o\}\\ \{\boldsymbol{P}^q_c\} + \{\tilde{\boldsymbol{Q}}_c\} + \{\boldsymbol{P}^p_c\}\end{Bmatrix}, \tag{27}$$

$$\begin{bmatrix}[\mathbf{F}_{cc}] & [\mathbf{F}_{ca}]\\ [\mathbf{F}_{ac}] & [\mathbf{F}_{aa}]\end{bmatrix}\begin{Bmatrix}\{\boldsymbol{p}_c\}\\ \{\boldsymbol{p}_a\}\end{Bmatrix} = \begin{bmatrix}[\mathbf{G}_{cc}] & [\mathbf{G}_{ca}]\\ [\mathbf{G}_{ac}] & [\mathbf{G}_{aa}]\end{bmatrix}\begin{Bmatrix}\{\boldsymbol{p}_{nc}\}\\ \{\boldsymbol{p}_{na}\}\end{Bmatrix} + \begin{Bmatrix}\{\boldsymbol{\Psi}_c\}\\ \{\boldsymbol{\Psi}_a\}\end{Bmatrix}, \tag{28}$$

where subscripts o, c, and a denote quantities corresponding to surfaces Γ_o, Γ_c, and Γ_a, respectively; $\{\boldsymbol{P}^q_o\}$ and $\{\boldsymbol{P}^q_c\}$ are the portions of the load vector due to applied mechanical loads; and $\{\boldsymbol{P}^p_c\}$ is the load vector resulting from the interaction with the enclosed fluid. The load vector $\{\boldsymbol{P}^p_c\}$ for the finite element, e, due to acoustic pressures on the interface is calculated as

$$\{\boldsymbol{P}^p_e\} = \int_{\Gamma_e} [\mathbf{N}]^{\mathrm{T}} p\{\mathbf{n}\}\,\mathrm{d}\Gamma, \tag{29}$$

where $[\mathbf{N}]$ is the matrix of interpolation functions. Within each finite element, e, the acoustic pressure is approximated in terms of nodal values as

$$p = \{\boldsymbol{N}\}^{\mathrm{T}}\{\boldsymbol{p}_e\}, \tag{30}$$

where the interpolation functions $\{\boldsymbol{N}\}$ are the same as those used in the boundary element discretization. Equation (30) is introduced into equation (29) to obtain

$$\{\boldsymbol{P}^p_e\} = [\mathbf{R}_e]\{\boldsymbol{p}_e\}, \tag{31}$$

where the element matrix $[\mathbf{R}_e]$ is given as

$$[\mathbf{R}_e] = \int_{\Gamma_e} [\mathbf{N}]^{\mathrm{T}}\{\boldsymbol{n}\}\{\boldsymbol{N}\}^{\mathrm{T}}\,\mathrm{d}\Gamma. \tag{32}$$

A standard finite element assembly procedure is followed to obtain the expression for the load vector $\{\boldsymbol{P}^p_c\}$ in terms of acoustic pressures on the interface as

$$\{\boldsymbol{P}^p_c\} = [\mathbf{R}]\{\boldsymbol{p}_c\}. \tag{33}$$

An additional set of relations is obtained by using the compatibility of fluid and shell displacements on the interface. The normal derivative of the fluid pressure is related to the structural displacements by the relation [25]

$$p_n = \rho_f \omega^2 u_n, \tag{34}$$

where $u_n = \{\boldsymbol{u}\}^{\mathrm{T}} \cdot \{\boldsymbol{n}\}$ and ρ_f is the mass density of the fluid. Relation (34) is written for all nodes on the interface to obtain

$$\{\boldsymbol{p}_{nc}\} = \rho_f \omega^2 [\mathbf{n}] \{\boldsymbol{U}_c\}, \tag{35}$$

where $[\mathbf{n}]$ is the matrix that contains components of the outward normal vectors at the appropriate boundary element nodes.

The interface relations given in equations (33) and (35) are introduced into shell and fluid systems of equations (27) and (28) to obtain the equations for the coupled system

$$\begin{bmatrix} [\mathbf{K}^*_{oo}] & [\mathbf{K}^*_{oo}] & [\mathbf{0}] & [\mathbf{0}] \\ [\mathbf{K}^*_{co}] & [\mathbf{K}^*_{cc}] & -[\mathbf{R}] & [\mathbf{0}] \\ [\mathbf{0}] & [\mathbf{G}^n_{cc}] & [\mathbf{F}_{cc}] & [\mathbf{F}_{ca}] \\ [\mathbf{0}] & [\mathbf{G}^n_{ac}] & [\mathbf{F}_{ac}] & [\mathbf{F}_{aa}] \end{bmatrix} \begin{Bmatrix} \{\boldsymbol{U}_o\} \\ \{\boldsymbol{U}_c\} \\ \{\boldsymbol{p}_c\} \\ \{\boldsymbol{p}_a\} \end{Bmatrix} = \begin{Bmatrix} \{\boldsymbol{P}^q_o\} + \{\tilde{\boldsymbol{Q}}_o\} \\ \{\boldsymbol{P}^q_c\} + \{\tilde{\boldsymbol{Q}}_c\} \\ [\mathbf{G}_{ca}]\{\boldsymbol{p}_{na}\} + \{\boldsymbol{\Psi}_c\} \\ [\mathbf{G}_{aa}]\{\boldsymbol{p}_{na}\} + \{\boldsymbol{\Psi}_a\} \end{Bmatrix}, \tag{36}$$

where $[\mathbf{G}^n_{ac}] = \rho_f \omega^2 [\mathbf{G}_{ac}][\mathbf{n}]$ and $[\mathbf{G}^n_{aa}] = \rho_f \omega^2 [\mathbf{G}_{aa}][\mathbf{n}]$.

5. NUMERICAL STUDIES

Numerical studies have been performed in order to evaluate the formulations developed in this study. Formulations for the analysis of smart structures and for the acoustic response were first verified separately. Reference [12] provides comparisons of the shell element with an exact solution for piezoelectric plates, and a three-dimensional formulation developed in reference [29]. The boundary element formulation for three-dimensional acoustics was individually tested for three distinct problems with available analytical solutions: (1) one-dimensional motion, (2) vibrations of a long circular cylinder, and (3) radial motion of a pulsating sphere. Excellent agreement with the analytical solutions was achieved with a small number of boundary elements [30]. The coupled responses of the composite shell and the enclosed fluid are evaluated through extensive convergence studies of both structural and fluid variables. Finally, responses for various load cases are provided in order to demonstrate the capabilities of the present developments.

5.1. COUPLED ANALYSIS OF THE PIEZOELECTRIC SHELL AND THE ENCLOSED FLUID

The validity of the formulation for the coupled smart structure-acoustic fluid response and its capabilities are demonstrated by analyzing the circular cylindrical shell shown in Figure 2(a). The geometric configuration of the shell is described in a cylindrical co-ordinate system, and is defined by the inner radius, $r_i = 0{\cdot}289$ m, the outer radius, $r_o = 0{\cdot}293$ m, and the height, $h = 0{\cdot}3048$ m. The shell consists of an inner layer made of titanium, and an outer piezoelectric layer made of PZT4 with material properties given in Table 1. The interface between the layers is defined by radius $r_c = 0{\cdot}292$ m. The shell encloses air with mass density $\rho_a = 1{\cdot}12$ kg/m^3 and $c = 344{\cdot}4$ m/s^2. The coupled response is obtained for both mechanical loadings and the applied electric potentials. The mechanical loading consists of a line load $q = \bar{q}\, \mathrm{e}^{\mathrm{i}\omega t}$, as shown in Figure 2(a). Three distinct sets of electric potentials $\phi(z, \theta, t) = \phi(\theta)\, \mathrm{e}^{\mathrm{i}\omega t}$ applied on the outer surface of the

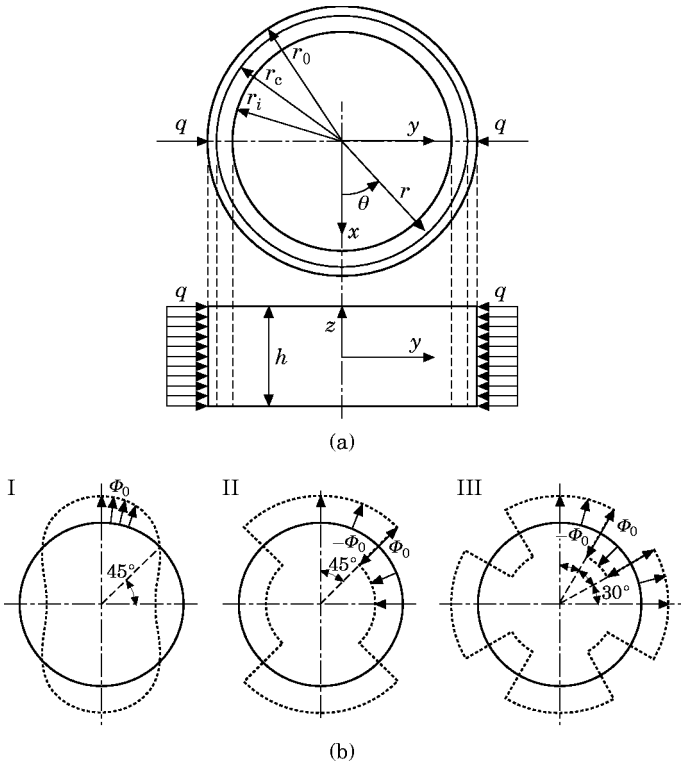

Figure 2. Cylindrical shell: (a) geometry, (b) applied electric potential.

TABLE 1

Material properties of the cylindrical shell

Property	Titanium	PZT-4
Elastic (GPa)		
E_{11}	114·0	81·3
E_{22}	114·0	81·3
E_{33}	114·0	64·5
E_{23}	43·8	25·6
E_{31}	43·8	25·6
E_{12}	43·8	30·4
v_{12}	0·3	0·33
v_{23}	0·3	0·43
v_{31}	0·3	0·43
Peizoelectric coefficients (10^{-2}) m/V)		
d_{31}	0·0	−122·0
d_{32}	0·0	−122·0
d_{24}	0·0	495·0
d_{15}	0·0	495·0
Electric permittivities		
$\varepsilon_{11}/\epsilon_o$	1475·0	1475·0
$\varepsilon_{11}/\epsilon_o$	1475·0	1475·0
$\varepsilon_{11}/\epsilon_o$	1475·0	1300·0
Mass Density (kg/m^3)		
ρ	2768·0	7600·0

$\varepsilon_o = 8{\cdot}85 \times 10^{-12}$ F/m—electric permittivity of the air

TABLE 2

Description of load cases for coupled analysis

Load	Mechanical	Applied electric potentials	
Case	Load	Layer interface	Outer surface
A	line load	zero	zero
B	line load	zero	–
C	none	zero	case I
D	none	zero	case II
E	none	zero	case III

active material are considered. The circumferential amplitude variations, $\phi(\theta)$, of the applied electric potentials are shown in Figure 2(b), and include a sinusoidal variation $\phi(\theta) = \phi_o \cos(\theta)$ (Case I) and two alternating uniform voltage patterns (Cases II and III). The amplitude of the line load is $\bar{q} = 656$ N/m, and the reference value of the applied electric potential is $\phi_o = 100$ V. The above mechanical loads and electric potentials are combined to define five distinct load cases, as summarized in Table 2. For all load cases, the electric potentials in the piezoelectric layer interface are set to zero. It is noted that the difference between the load cases A and B is that in the case A all the electric potentials on the outer surface are prescribed to zero (closed circuit conditions) while in the case B the electric potentials on the outer surface remain free (open circuit conditions).

The structure and the applied external influences are symmetric with respect to all three co-ordinate axes and only one octant of the shell, $0 \leqslant \theta \leqslant 90^\circ$, $0 \leqslant z \leqslant h/2$, and the corresponding portion of the enclosed fluid domain are modelled. The portions of the fluid and structure domains that are considered in the analysis are discretized using boundary and finite elements, respectively, as shown in Figure 3. The shell surface is discretized using L eight-node finite elements. Three electric potentials are defined for each node (N = 3): on the inner and outer contours, respectively, and on the layer interface. The interface portion of the fluid boundary is discretized with L quadratic conforming boundary elements, using the same nodes that are employed in the finite element discretization of the cylindrical shell. The portions of the fluid boundary that lie on the plates $z = 0$ and $z = h/2$ are discretized using $1{\cdot}5L$ boundary elements, as shown in Figure 3, while two boundary elements are used for the planes of symmetry, $x = 0$ and $y = 0$. Appropriate boundary conditions are applied at nodes lying on the planes of symmetry. A two-dimensional fluid motion is imposed, without loss of generality, by prescribing fluid boundary conditions $p_n = 0$ on the planes $z = 0$ and $z = h/2$.

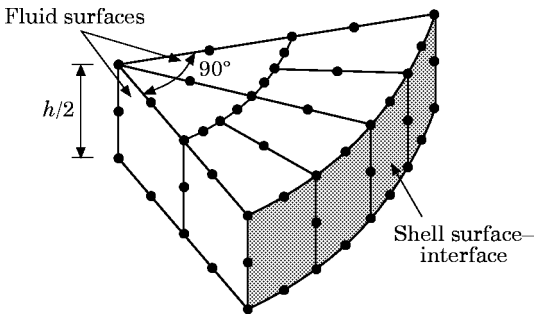

Figure 3. Finite/boundary element discretization of the shell and the enclosed fluid.

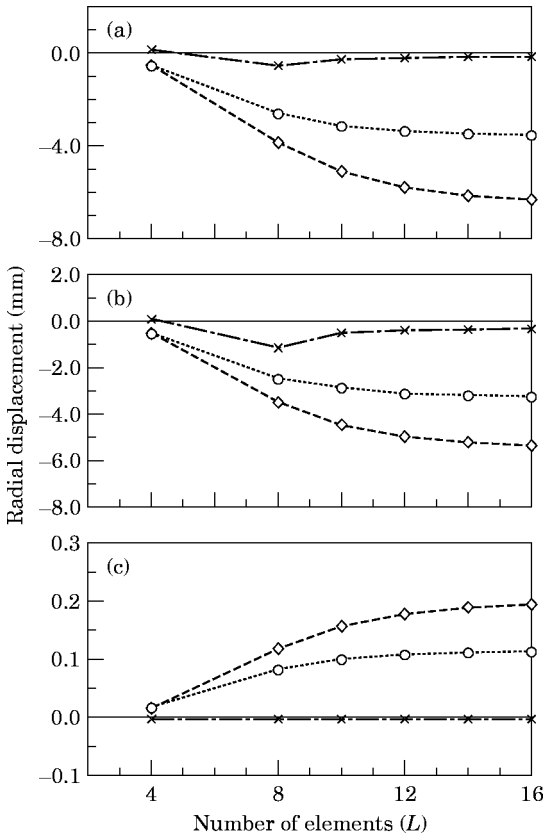

Figure 4. Convergence of radial displacement w at $\theta = 0^\circ$ at various forcing frequencies: (a) load case A; (b) load case B; (c) load case C. ···○···, 0 Hz; - -◇- -, 20 Hz; ·–×–·, 200 Hz.

Convergence studies of the response variables are performed for the load cases A, B, and C for various excitation frequencies. The convergence of the radial displacement w at $\theta = 0^\circ$ on the fluid-structure boundary is shown in Figure 4, and the convergence of the acoustic pressure p at the same location in Figure 5. The convergence of the sensory electric potentials ϕ in the piezoelectric material for the load case B is demonstrated in Figure 6. It is seen from Figures 4–6 that fast convergence of the response variables is achieved with the present formulation. A somewhat larger number of elements on the interface is required, as expected, for higher excitation frequencies. The zero frequency denotes the corresponding static response. The non-monotonic convergence at 200 Hz is due to the overestimation of the second modal frequency with low mesh densities, which is very close to this excitation frequency. The differences in the predicted amplitudes of the radial displacements and acoustic pressures for load cases A and B that involve open and closed circuit conditions, respectively, indicate the effect of electric boundary conditions on the response of the cylinder.

The frequency response of the radial displacements and the acoustic pressures at $\theta = 0^\circ$ for the load cases A, C, and B are shown in Figures 7 and 8, respectively. Also shown in Figure 8 is the frequency response of the sensory electric potential at $\theta = 0^\circ$ for the load case B. The results are obtained for three finite element discretizations consisting of $L = 12$, 14, and 16 elements. The location of the resonance frequencies of the coupled system is obvious in Figures 7 and 8.

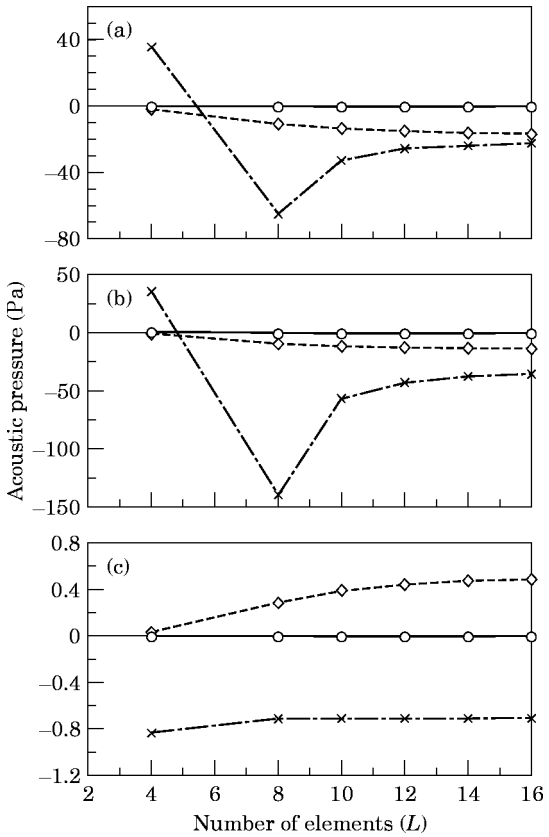

Figure 5. Convergence of acoustic pressure p at $\theta = 0^\circ$ for various forcing frequencies: (a) load case A; (b) load case B; (c) load case C. ···○···, 0 Hz; - -◇- -, 20 Hz; ·–×·–, 200 Hz.

The distribution of radial displacements on the interface and acoustic pressures inside the cylinder are considered next. The predicted amplitudes of the radial displacement for the load cases A, C, D, and E are shown in Figure 9. The lines shown in Figure 9(a–d) depict deformed shapes of the reference surface of the shell. The internal distributions of acoustic pressures are shown in Figure 10 for the load case A, and in Figure 11 for the load case E. The applied potential pattern in the load case E approximates the modal

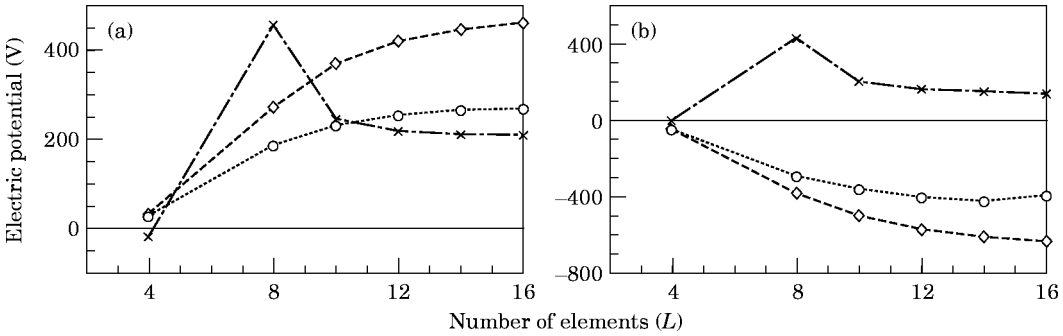

Figure 6. Convergence of sensory electric potential for the load case B for various forcing frequencies: (a) at $\theta = 0^\circ$, (b) at $\theta = 90^\circ$. ···○···, 0 Hz; - -◇- -, 20 Hz; –·–×·–·–, 200 Hz.

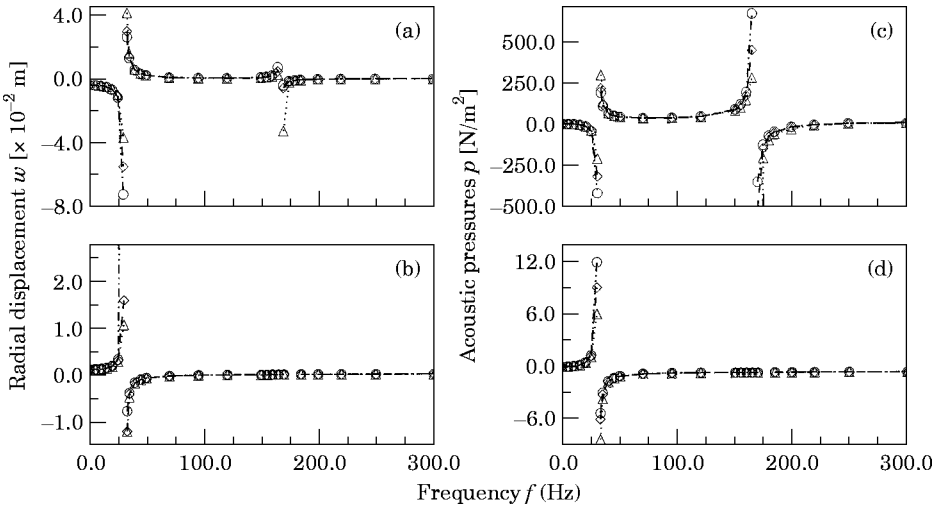

Figure 7. Frequency response of state variables (real component) at $\theta = 0^\circ$ for load cases A and C. (a) Radial displacement—load case A; (b) radial displacement—load case C; (c) acoustic pressure—load case A; (d) acoustic pressure—load case C. ···△···, $L = 12$; - -◇- -, $L = 14$; ·–○·–, $L = 16$.

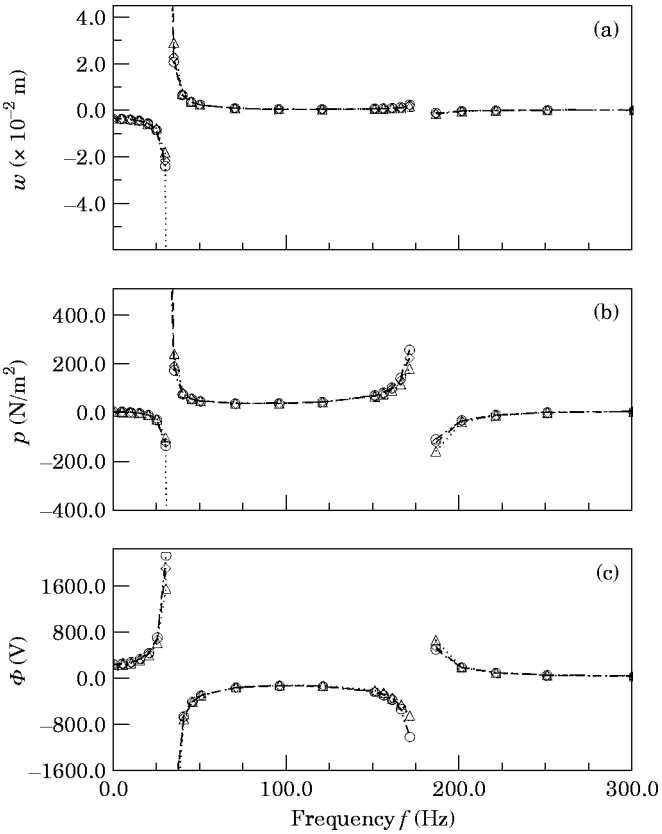

Figure 8. Frequency response of state variables (real component) at $\theta = 0^\circ$ for load case B. (a) Radial displacement w; (b) acoustic pressure p; (c) sensory electric potential Φ. ···△···, $L = 12$; - -◇- -, $L = 14$; ·–○·–, $L = 16$.

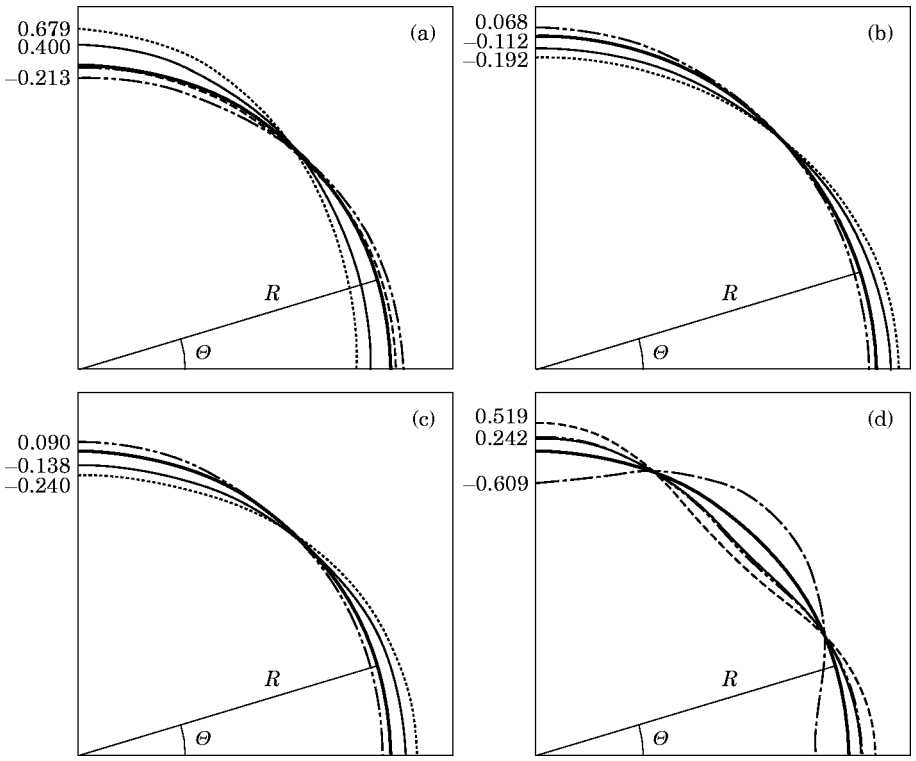

Figure 9. Radial deflection (in mm) of the shell for various excitation frequencies. (a) load case A; (b) load case C; (c) load case D; (d) load case E. ——, 0 Hz; ····, 20 Hz; ·—··—··, 50 Hz; - - - -, 120 Hz; —·—·, 200 Hz.

voltage distribution of the second vibration mode. It is seen from Figures 10 and 11 that the distribution pattern of the internal pressure for the load case A changes with the excitation frequency of the mechanical load, while it remains the same for the load case E. It may, therefore, be concluded that the stepwise distribution of the applied electric potential excites only one mode thus resulting in the same internal pressure distribution. Such an information may be very useful in the application of the present developments in problems of noise reduction and vibration control. As seen from the above results, the

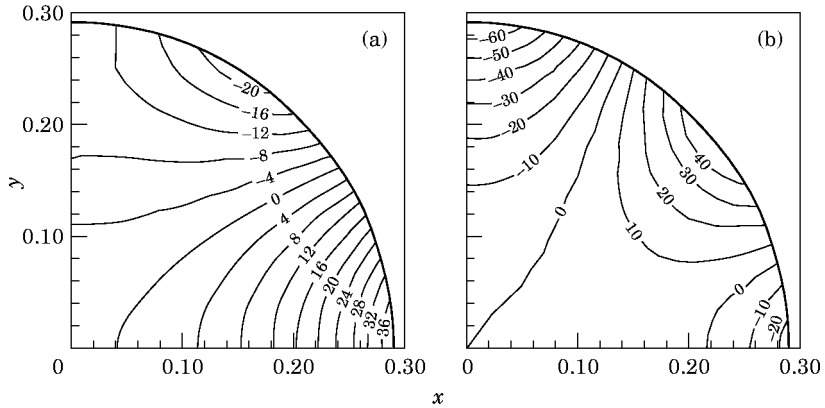

Figure 10. Distribution of the acoustic pressure on the plane z = 0·0762 m for load case A. (a) Excitation frequency at 120 Hz; (b) excitation frequency at 200 Hz. Pressure units are in Pa, length units in m.

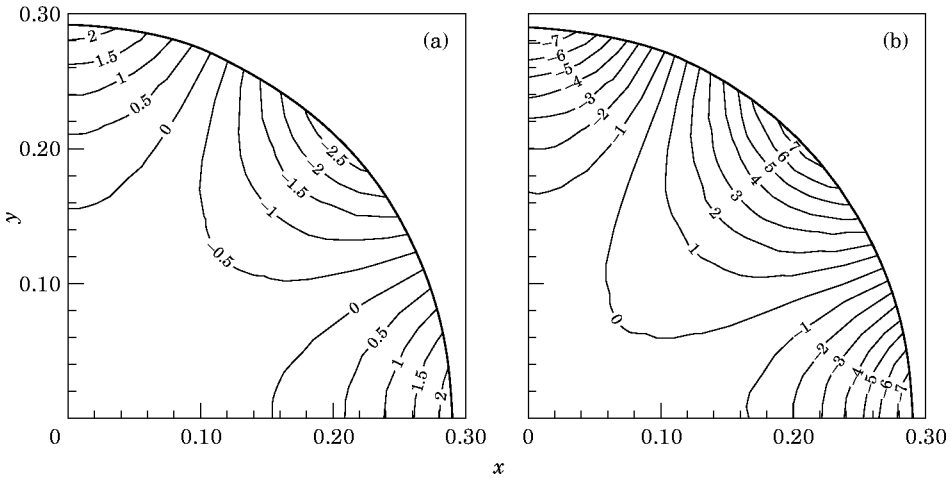

Figure 11. Distribution of the acoustic pressure on the plane z = 0·0762 m for load case E. (a) Excitation frequency at 120 Hz; (b) excitation frequency at 200 Hz. Pressure units are in Pa, length units in m.

motion of the structure and the induced acoustic field may be affected by changing the intensity of the applied electric potentials as well as the spatial distribution of actuators and/or applied voltage patterns.

6. SUMMARY

A formulation to calculate the coupled response of smart composite shell structures and the enclosed acoustic fluid has been presented. The mixed-field piezoelectric shell theory and the corresponding finite element were employed to model smart composite structures. The shell theory treated both mechanical displacements and electric potentials as unknown variables and was applicable to shells of arbitrary shapes, multi-layer configurations and general sensory or active arrangements of piezoelectric layers. A three-dimensional boundary element formulation was developed to calculate the acoustic response of the enclosed fluid. Quadratic conforming boundary elements were used to discretize the fluid boundary. Advanced numerical integration techniques were used to calculate singular integrals in the boundary element matrices. The treatment of the distributed acoustic sources was also presented. The two formulations above were next combined for the analysis of the coupled problem. Relations between the structural and acoustic variables were utilized to develop the coupling equations. The final system of equations was obtained in terms of the mechanical displacements of the shell and the acoustic pressures on the fluid boundary. After solving the system of equations for the unknown variables, the sensory electric potentials were calculated using the condensation relations. The acoustic pressures inside the fluid domain, if required, were calculated using the corresponding boundary values. The validity of the present developments was established. The formulations for the analysis of piezoelectric shells and for the acoustic response of the fluid were first verified separately, by comparing the results with those obtained from alternative numerical techniques and analytical solutions where available. The formulation for the coupled response was evaluated next by performing convergence studies of the response variables for a variety of applied external influences. Finally, capabilities of the present developments were demonstrated.

The present formulation represents a formidable analysis tool. The coupled response was obtained for arbitrary external influences, including mechanical loadings, applied electric potentials, and distributed acoustic sources. The mixed field theory for the analysis of composite piezoelectric shells and the boundary element formulation for the acoustic response of the enclosed fluid result in computationally efficient and economic computations, as was demonstrated by convergence studies and other numerical results. It was shown that applied electric potentials in the piezoelectric actuators induce shell vibrations, as well as acoustic pressures in the fluid. It was also demonstrated that the acoustic pressure field can be controlled by the pattern and intensity of applied electric potentials, as well as by the distribution of piezoelectric acuators. It may, therefore, be concluded that the present developments represent a solid analytical basis for subsequent studies on noise monitoring, noise reduction and vibration control.

ACKNOWLEDGMENTS

This work has been supported by grant NAS3-27804 and co-operative agreement C-NCC3-391 from Structural Mechanics Branch, NASA Lewis Research Center in Cleveland, Ohio. Mr. Dale Hopkins has been the project manager. This support is gratefully acknowledged.

REFERENCES

1. C. R. Fuller and J. D. Jones 1987 *Journal of Sound and Vibration* **112**, 389–395. Experiments on reduction of propeller induced interior noise by active control of cylinder vibration.
2. R. H. Thomas, R. A. Burdisso, C. R. Fuller and F. O'Brien 1993 *Journal of Sound and Vibration* **161**, 532–537. Preliminary experiments on active control of fan noise from a turbofan engine.
3. B. Balachandran, A. Sampath and J. Park submitted to *Smart Materials and Structures*. Active control of interior noise in a three-dimensional structure.
4. J. Pan, C. H. Hansen and D. A. Bies 1990 *Journal of Acoustical Society of America* **87**, 2098–2108. Active control of noise transmission through a panel into a cavity: I. Analytical study.
5. S. Koshigoe, J. T. Gillis and E. T. Falangas 1993 *Journal of Acoustical Society of America* **94**, 900–907. A new approach for active control of sound transmission through an elastic plate backed by a rectangular cavity.
6. H. S. Tzou and M. Gadre 1989 *Journal of Sound and Vibration* **132**, 433–450. Theoretical analysis of a multi-layered thin shell coupled with piezoelectric shell actuators for distributed vibration controls.
7. H. S. Tzou and R. V. Howard 1994 *Journal of Vibration and Acoustics* **116**, 295–302. A piezothermoelastic thin shell theory applied to active structures.
8. H. S. Tzou and J. P. Zhong 1993 *Journals of Dynamic Measurement and Control Systems* **115**, 506–517. Electromechanics and vibrations of piezoelectric shell distributed systems.
9. P. H. Larson and J. R. Vinson 1993 *ASME Winter Annual Meeting*, New Orleans. The use of piezoelectric materials in curved beams and rings.
10. P. R. Heyliger, G. Ramirez and K. C. Pei 1994 *Technical report* 195383, *NASA Lewis Research Center*, *Cleveland*, *Ohio*. Discrete-layer piezoelectric plate and shell models for active tip-clearance control.
11. H. S. Tzou and R. Ye 1996 *American Institute of Aeronautics and Astonautics* **34**, 110–115. Analysis of piezoelastic structures with laminated piezoelectric triangle shell elements.
12. D. A. Saravanos 1996 *Technical Report CR*-198490, *NASA Lewis Research Center*, *Cleveland*, *OH*. Coupled mixed-field laminate theory and finite element for smart piezoelectric composite shell structures.
13. J. N. Reddy 1989 *International Journal for Numerical Methods in Engineering* **27**, 361–382. On refined computational models of composite laminates.

14. P. K. Banerjee and R. Butterfield 1981 *Boundary Element Method in Engineering Science*. Maidenhead, England: McGraw-Hill.
15. J. C. Lachat and J. O. Watson 1976 *International Journal for Numerical Methods in Engineering* **10**, 991–1005. Effective numerical treatment of boundary integral equations: A formulation for three–dimensional elastostatics.
16. I. Kaljević and S. Saigal 1995 *Computer Methods in Applied Mechanics and Engineering* **121**, 211–230. Stochastic boundary elements for two-dimensional potential flow in non-homogenous media.
17. D. A. Pape and P. K. Banerjee 1987 *ASME Journal of Applied Mechanics* **54**, 866–871. Treatment of body forces in 2D elastostatics BEM using particular integrals.
18. D. P. Henry and P. K. Banerjee 1988 *International Journal for Numerical Methods in Engineering* **26**, 2061–2077. A new boundary element formulation for two- and three-dimensional thermoelasticity using particular integrals.
19. B. Mariem and M. A. Hamdi 1987 *International Journal for Numerical Methods in Engineering* **24**, 1251–1267. A new boundary finite element method for fluid/structure interaction.
20. G. C. Everstine and F. M. Henderson 1990 *Journal of Acoustical Society of America* **87**, 1938–1947. Coupled finite element/boundary element approach for fluid–structure interaction.
21. I. C. Mathews 1986 *Journal of Acoustical Society of America* **79**, 1317–1325. Numerical techniques for three-dimensional steady-state fluid-structure interaction.
22. R. A. Jeans and I. C. Mathews 1990 *Journal of Acoustical Society of America* **88**, 2459–2456. Solution of fluid structure interaction problem using a coupled finite element and variational boundary element technique.
23. C. Rajakumar, A. Ali and S. M. Yunus 1992 *International Journal for Numerical Methods in Engineering* **33**, 369–386. A new acoustic interface element for fluid–structure interaction problems.
24. H. F. Tiersten 1969 *Linear Piezoelectric Plate Vibrations*. New York: Plenum Press.
25. A. D. Pierce 1989 *Acoustics*: *An Introduction to its Physical Principles and Applications*. Woodbury, New York: Acoustical Society of America.
26. B. B. Baker and E. T. Copson 1950 *The Mathematical Theory of Heygens' Principle*. Oxford: Clarendon Press, second edition.
27. S. Ahmad and P. K. Banerjee 1987 *International Journal for Numerical Methods in Engineering* **26**, 1709–1721. Time-domain transient elastodynamic analyses of 3-D solids with BEM.
28. A. S. M. Israil and P. K. Banerjee 1990 *International Journal for Numerical Methods in Engineering* **29**, 1421–1440. Advanced time-domain BEM for two-dimensional problems in elastodynamics.
29. P. Heyliger, K. C. Pei and D. Saravanos *American Institute of Aeronautics and Astonautics Journal* in press. Layerwise mechanics and finite element model for laminated piezoelectric shells.
30. I. Kaljević and D. Saravanos *Technical report*, *NASA Lewis Research Center*, *Cleveland*, *Ohio*, in press. Coupled analysis of smart composite shell structures surrounding acoustic enclosures.